ACS OMEGA

Article

Cite This: ACS Omega 2019, 4, 3790−3799

http://pubs.acs.org/journal/acsodf

Magnetic One-Step Purification of His-Tagged Protein by Bare Iron Oxide Nanoparticles

Sebastian P. Schwaminger,*[,†,§,∥] Paula Fraga-García,*[,†,∥] Silvia A. Blank-Shim,[†] Tamara Straub,[†] Martin Haslbeck,[‡] Francesco Muraca,[§] Kenneth A. Dawson,[§] and Sonja Berensmeier*[,†]

[†]Bioseparation Engineering Group, Department of Mechanical Engineering and [‡]Department of Chemistry, Technical University of Munich, Garching 85748, Germany

[§]Centre for BioNano Interactions, School of Chemistry and Chemical Biology and Conway Institute for Biomolecular and Biomedical Research, University College Dublin, Belfield, Dublin D14 YH57, Ireland

Supporting Information

ABSTRACT: Magnetic separation is a promising alternative to conventional methods in downstream processing. This can facilitate easier handling, fewer processing steps, and more sustainable processes. Target materials can be extracted directly from crude cell lysates in a single step by magnetic nanoadsorbents with high-gradient magnetic fishing (HGMF). Additionally, the use of hazardous consumables for reducing downstream processing steps can be avoided. Here, we present proof of principle of one-step magnetic fishing from crude *Escherichia coli* cell lysate of a green fluorescent protein (GFP) with an attached hexahistidine (His_6)-tag, which is used as the model target molecule. The focus of this investigation is the upscale to a liter scale magnetic fishing process in which a purity of 91% GFP can be achieved in a single purification step from cleared cell lysate. The binding through the His_6-tag can be demonstrated, since no significant binding of nontagged GFP toward bare iron oxide nanoparticles (BIONs) can be observed. Nonfunctionalized BIONs with primary particle diameters of around 12 nm, as used in the process, can be produced with a simple and low-cost coprecipitation synthesis. Thus, HGMF with BIONs might pave the way for a new and greener era of downstream processing.

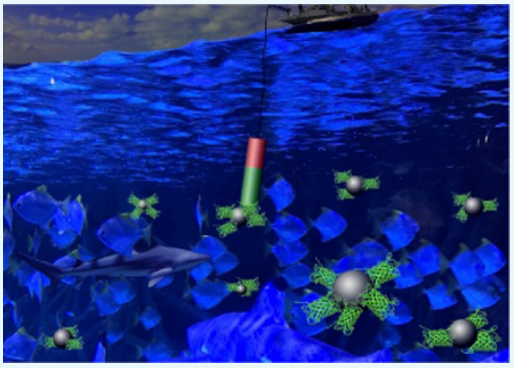

INTRODUCTION

In nature, multifarious interactions between biomolecules and inorganic surfaces occur, ranging from the adhesion of organisms under the sea to the growth of bones and teeth in vertebrates. The control of these interactions can be utilized to implement applications in nanomedicine for implant coatings,[1] drug delivery,[2] or magnetic resonance imaging.[3,4] Furthermore, with the help of a fundamental understanding of the interaction, new application fields emerge, ranging from biosensing,[5,6] (bio-)catalysis,[7,87,8] and power storage to wastewater treatment and toxicology,[9] as well as purification of therapeutic proteins.[10,11] To investigate these biointerfacial phenomena, the binding processes, parameters influencing the interactions, and protein organization at the surface need to be characterized thoroughly.[12] There are multiple possibilities to study, interpret, and apply interactions at bio−nano interfaces.[13−15] The main issue for all approaches is the interplay of many different forces and components in complex biological fluids, which control the interactions between biomolecules and nanomaterials. In complex fluids, the components (from small molecules to large proteins) define the surface of nanoparticles. This dynamic concept is called corona formation, and it occurs immediately in biological media.[16,17] Biomolecules are loosely bound to the surface and the composition is determined by biomolecules' incidence and affinity.[18−20] Particularly, superparamagnetic nanoparticles are of great interest, as their magnetic properties facilitate transport and magnetic sensing of biomolecules as well as magnetically induced heating.[21,22] Thus, many applications, especially in the medical sector, emerge from these magnetic nanomaterials.[23] However, their properties can be used in biotechnology,[24−28] catalysis,[7,29] and data storage.[30] One approach to control the interaction of magnetic nanoparticles with biomolecules is the tailoring of the particle surface by different modifications and functionalization methods.[21,22,26,31,32] This particle tuning not only affects the aqueous interface, and therefore the interaction with biomolecules, but also changes the stability of particles in suspension and thus the mechanical properties. Consequently, controlling the surface properties presents the greatest challenge in nanotechnology as not only surface modifications but also the buffer composition as well as detergents and biomolecules in complex media determine the identity of nanoparticles.[33−35]

Another aspect, which is difficult to control, is the agglomeration behavior of nanoparticles when exposed to

Received: November 30, 2018
Accepted: January 4, 2019
Published: February 21, 2019

DOI: 10.1021/acsomega.8b03348
ACS Omega 2019, 4, 3790−3799

biomolecules in complex media.[36] However, the agglomeration strongly affects the hydrodynamic properties and, accordingly, the ability to process magnetic nanoparticle fluids mechanically and magnetically. Low-cost magnetic nanoparticles, usually consisting of magnetite, maghemite, transition states in between, or mixtures of both materials, have to be smaller than 20−30 nm to possess superparamagnetic properties, which facilitate simple handling in separation due to no remanence at room temperature.[37]

Even though magnetic separation holds many advantages compared with standard processes and is already in use for medical applications, no industrial processes exist to date.[8,38]

On the other hand, several approaches to design and build industrially relevant high-gradient magnetic fishing (HGMF) separators do exist.[38,39] The models range from filler materials (such as iron spheres or steel wool over wires and meshes) to defined matrix structures. However, especially, the recovery of magnetic nanoparticles and the target molecules is a critical processing aspect, which can be solved with different approaches, including two-phase flow, sonication, or movable matrices such as a rotor−stator set-up.[38] For this investigation, a rotor−stator HGMF was used to achieve an easy and fast redispersion and deagglomeration of nanoparticles. Generally, especially small iron oxide nanoparticles tend to aggregate under ambient conditions and at high salt concentrations.[40] This effect is always strengthened in fields. As a result, agglomerations positively affect the hydrodynamic properties and thus the separation efficiencies, which is used for most applications of magnetic nanoparticles.[21,41] On the other hand, aggregation lowers the effective surface area of nanoparticles, and colloidal stability presents a major challenge in HGMF accordingly.

Here, we use completely nonfunctionalized bare iron oxide nanoparticles (BIONs), which are not very colloidally stable under ambient conditions without stabilizing molecules within a pH range of 5.5−8.5, but form large agglomerates at the microscale.[42,43] These particles are used as adsorbents for the purification of green fluorescent protein (GFP) that contains a hexahistidine (His_6)-tag commonly used in affinity chromatography downstream processing. We use the affinity of the histidine side chains, in the tag sequence, to the nanoscale iron oxide surface, which is composed of iron ions ligated by hydroxyl groups.[25,44] Here, a coordination to the iron ions and buffer-controlled electrostatic interactions leads to a preferential adsorption of His-tagged proteins, which can be magnetically separated. As a further processing step, the proteins can be released with an elution buffer similar to that used for immobilized metal-affinity chromatography (IMAC).[45] IMAC is a conventional process that is used in industry and on the lab scale for purification of several proteins. Metal ions are chelated by ligands that are attached to the chromatography resin.[46] Thus, the His-tag interacts with the chelated ions resulting in a reversible coordination bond. Therefore, this method can be used for affinity protein purification.[46] Some research groups already adapted the IMAC principle for magnetic separation processes.[41,47−50] However, the investigations are based on magnetic microparticles that are functionalized by linker chelating metal ions.[51] Even though the principle of His-tagged protein separation, presented here, is similar to IMAC, we want to emphasize that our particles are used as bare nanoparticles without surface modifications. In our process, the tag interacts with the particle surface via complexation and electrostatic interactions.[52,53] However, the iron ions at the aqueous interface are tightly bound to the BIONs and therefore do not leach. Consequently, neither expensive complexation agents nor toxic metal ions are required, since no regeneration is needed for the process presented here.[54] We focused on the upscaling of HGMF for industrially relevant processes and were able to validate the upscaling with a magnetic separation pilot plant in the liter scale.

RESULTS AND DISCUSSION

The properties of the BIONs synthesized via a coprecipitation synthesis used for all experiments were reported earlier in an investigation by our group.[55] BIONs demonstrate a sharp particle size distribution of around 12 nm, which was obtained by transmission electron microscopy (TEM) measurements (Figure S1). The small size of the nonfunctionalized nanoparticles leads to a large specific surface area of 89 $m^2 g^{-1}$ and superparamagnetic properties (remanence < 1 emu g^{-1}) with a high saturation magnetization of 83 emu g^{-1}. The amphiphilic nature of the oxide nanoparticles is demonstrated by the sigmoidal ζ-potential, which is negatively charged above and positively charged below the isoelectric point at pH 6.57. Furthermore, the particles can be identified as magnetite from Raman spectroscopy and X-ray diffraction (XRD) measurements (Figures S1 and S2).[55]

His_6-GFP, expressed in *Escherichia coli* BL21 (DE3), was purified with anion exchange chromatography (AEX) after cell lysis. AEX was followed by a polishing step with immobilized metal affinity chromatography (IMAC) and a purity of >99.9% was achieved before further use of the His_6-GFP (Figures S3, S5 and Table S4).

The adsorption isotherms of pure His_6-GFP and BIONs are illustrated in Figure 1A. Interestingly, all buffer conditions led to the adsorption of His_6-GFP and a similar binding capacity around 0.25 g g^{-1} and thus a similar surface coverage of around 40% (Table S6). However, the affinity can be adjusted by the variation of the buffer. A high affinity, indicated by a low K_D value, can be observed for acetate (0.01 g L^{-1}), Tris-buffered saline (TBS, 0.01 g L^{-1}), and tris(hydroxymethyl)-aminomethane (Tris, 0.03 g L^{-1}). Morpholino ethane sulfonic acid (MES) and phosphate buffers led to a moderate (0.05 g L^{-1}) and low affinity (0.1 g L^{-1}), respectively (Table S6). Besides surface complexation of iron oxides by phosphate ions, such effects are usually ascribed to changes in the surface tension of the solvent and the surface by the buffer ions.[34,52,56,57] Another interesting observation is the adsorption of a reference GFP without a tag, which does not tend to adsorb in Tris buffer, clearly indicating the contribution to the binding of the freestanding His_6 sequence of the barrel-shaped protein (Figure 1). The nontagged protein shows a significantly lower binding capacity (0.07 g g^{-1}) than the His_6-tagged species. Therefore, changes in the buffer composition around BIONs can be used to influence the binding affinity of His_6-tagged proteins, which enables control of the separation process. The high maximum load of proteins on the nanoparticles can easily compete with metal ion-immobilized nanomaterials and chromatography resins.[47] Even the affinity of His_6-tagged GFP to the BION surface is in a range similar to that of Ni^{2+}-immobilized materials.[41,47,58] Another interesting point in the interaction of proteins with colloids is the agglomeration behavior. Uncoated BIONs show a tendency to agglomerate under ambient conditions in most buffer systems.[40,59,60] Even though the nanoparticles form

DOI: 10.1021/acsomega.8b03348
ACS Omega 2019, 4, 3790−3799

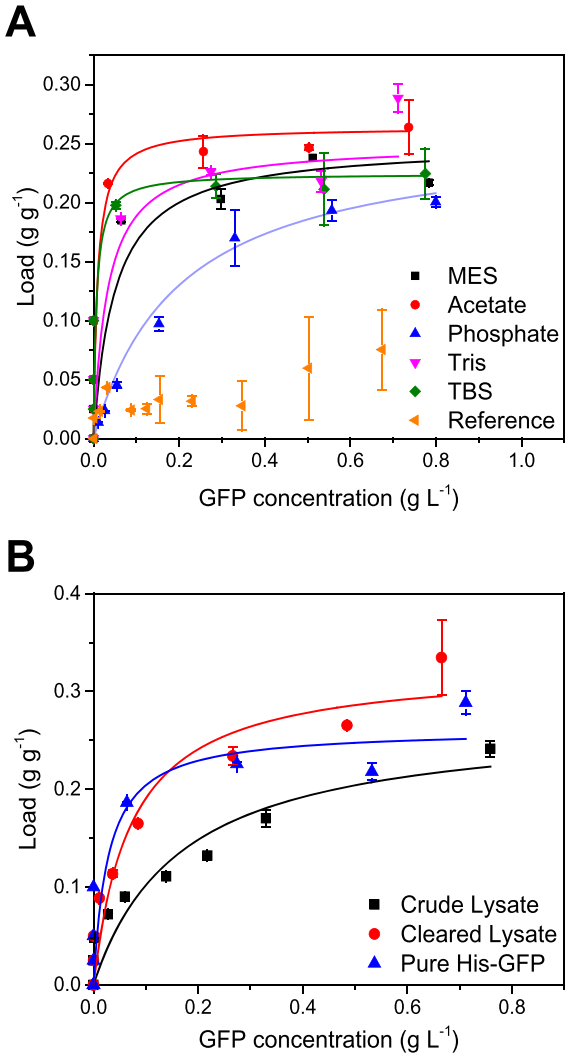

Figure 1. (A) Adsorption isotherms of His_6-GFP to BIONs in different buffer systems. All experiments contain 1 g L^{-1} BIONs with varying GFP concentrations. The GFP has a purity > 95% and the buffers at pH 7 contain 50 mM ions plus saline in case of TBS. The reference of nontagged GFP was conducted in Tris buffer. Error bars represent the standard deviation (±SD) of experiments in triplicate and the respective analyses in triplicate (nine measurements each). (B) Comparison of adsorption isotherms between pure His_6-GFP, cleared cell lysate containing no cell debris, and crude cell lysate in 50 mM Tris buffer with 1 g L^{-1} BIONs. Error bars represent the standard deviation (±SD) of experiments in duplicate and the respective analyses in triplicate (six measurements each).

agglomerates of up to 10 μm (Figure S7), we obtain this high binding capacity of His_6-GFP. This means that proteins are able to diffuse into the loosely bound agglomerates and bind to single particles or significantly smaller aggregates. In an earlier study, we observed a similar behavior of GFP containing a different tag binding to BIONs with small-angle neutron scattering.[61] Hence, these agglomerations provide the advantages of nano- and microparticles. This behavior is also visible in the different results from differential centrifugal sedimentation and optical centrifugation with hydrodynamic diameters below 100 nm compared with larger agglomerates, which can be observed by dynamic light scattering (Figure S7). Although these particles demonstrate the high specific surface area of small nanoparticles, their hydrodynamic properties are similar to those of large microparticles, leading to a fast separation in a high-gradient magnetic fishing process.[38,39,51,61] The binding capacity of His_6-GFP is furthermore not significantly affected by the presence of complex media such as the lysate from the *E. coli* fermentation broth (Figure 1B). The high affinity of His_6-GFP to the BION surface is still very high for cleared cell lysate where the cell debris is filtered prior to incubation with nanoparticles. Here, a moderately higher binding capacity can also be reached (0.33 g g^{-1}) under the same buffer conditions (50 mM Tris buffer at pH 7). This slight difference can be explained by an improved accessibility of nanoparticles in the complex suspension, protein−protein interactions, and co-adsorption processes. His_6-GFP adsorption to BIONs can also be observed in the lysate still containing cell debris even though with a lower affinity. Here, the same binding capacity to BIONs as for pure His_6-GFP can be reached. However, a high affinity of magnetic nanoparticles to cell walls of different organisms is assumed.[24,27,47] Hence, our adsorption experiments indicate that His_6-GFP selectively binds to the BION surface, which is the basis for an efficient separation process.

For purification processes, the recovery of target molecules is often difficult and more time sensitive than the separation and thus should be investigated thoroughly. Therefore, we compared different elution possibilities. As the binding should be mainly through the histidine tag, a reasonable possibility for elution is the change of electrostatic properties by a pH shift that can deprotonate or protonate the surface as well as the His_6-tag. Another strategy is the replacement of coordinative bonds of histidine subunits to iron ions by imidazole molecules and the weakening of electrostatic interactions by the introduction of a higher ionic strength with sodium and chloride ions.[34,62] Imidazole is commonly used as an eluent by replacing histidine side chains due to a similar coordination to metal ions for purification processes of His-tagged proteins with IMAC. Therefore, several buffers with focus on different imidazole concentrations are compared for their elution ability and summarized in Figure 2. The incubation of His_6-GFP with BIONs was conducted in Tris buffer at pH 7 and a pH shift to pH 9 or 5 leads to two completely different results. Although around 60% of the previously adsorbed GFP is eluted with a pH shift to basic environments, no protein elution can be observed for a pH shift toward the acidic region. The buffer leading to the lowest affinity of His_6-GFP to BIONs

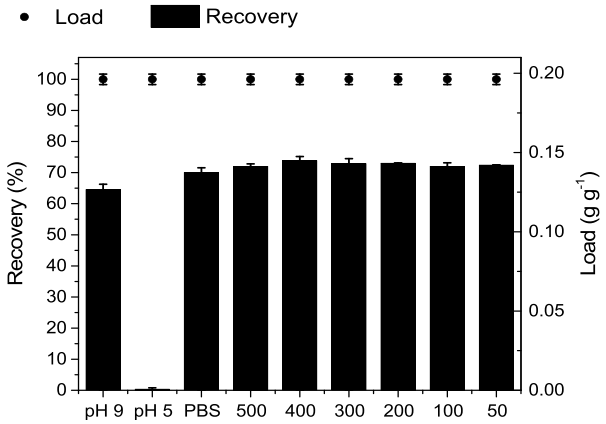

Figure 2. Elution of His_6-GFP with different buffers (TBS 50 mM at pH 9 and 5, PBS pH 7.4, and imidazole IMAC buffer pH 7.5: 500, 400, 300, 200, 100, and 50 mM).

DOI: 10.1021/acsomega.8b03348
ACS Omega 2019, 4, 3790−3799

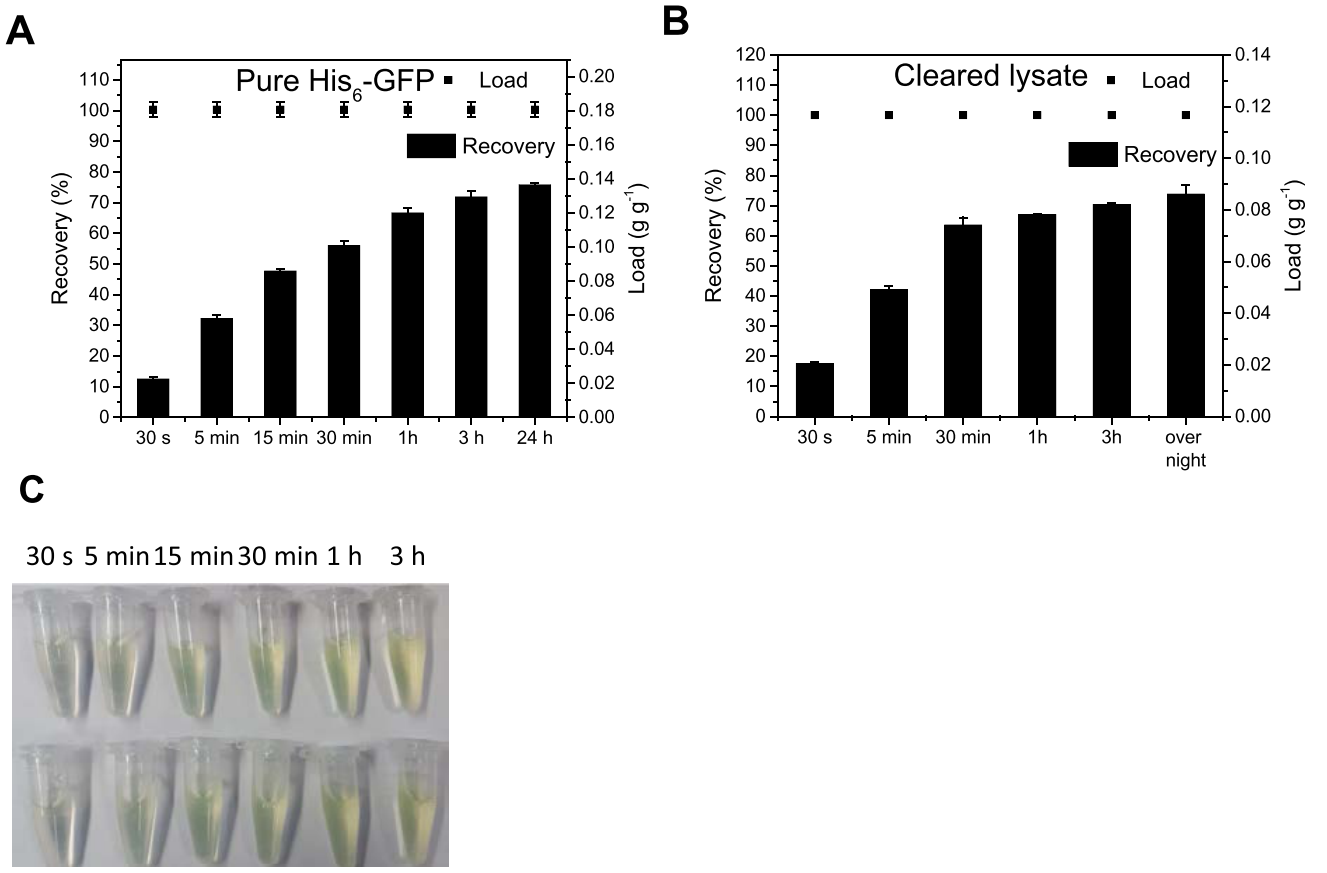

Figure 3. Elution kinetics of (A) pure His_6-GFP with 50 mM imidazole IMAC buffer pH 7.5 and (B) His_6-GFP from cleared lysate with 50 mM imidazole IMAC buffer pH 7.5 at different times. (C) Visualization of GFP elution over time.

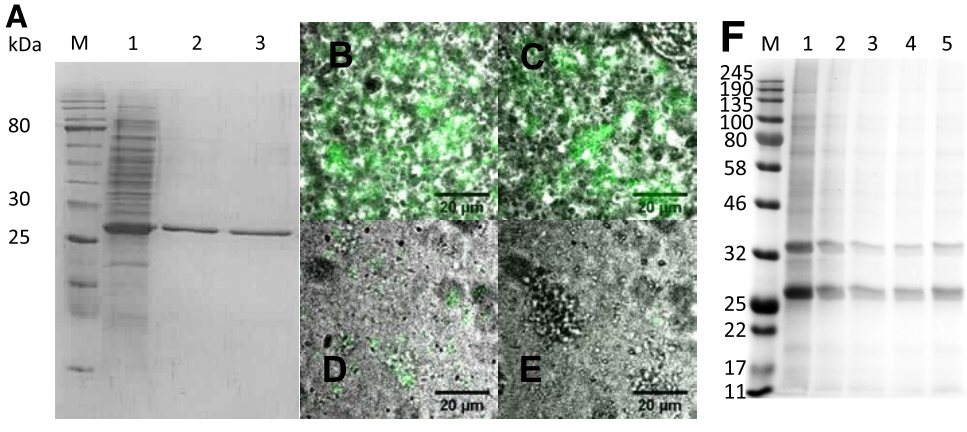

Figure 4. (A) SDS-gel of elution of proteins from cleared cell lysate incubated with 1 g L^{-1} BIONs: M (marker: unstained protein marker, broad range (2−212 kDa)), 1 (cleared cell lysate containing 0.25 g L^{-1} His_6-GFP), 2 (elution with 50 mM imidazole IMAC buffer pH 7.5), and 3 (elution with 500 mM imidazole IMAC buffer pH 7.5). Fluorescence microscopy and the overlay light microscopy image with excitation at 488 nm and emission at 520 nm of BIONs. (B) BIONs 1 g L^{-1} after incubation with cleared cell lysate containing 1 g L^{-1} GFP in 50 mM Tris buffer pH 7 after a washing step with the same buffer. (C) BIONs after a second washing step. (D) BIONs after elution with 500 mM imidazole IMAC buffer pH 7.5. (E) Reference of nontagged GFP after one washing step. (F) SDS-PAGE of the protein corona formed after interaction of the lysate proteins with the BIONs. M (color protein standard broad range (10−250 kDa)), 1 (corona after first wash), 2 (corona after second wash), 3 (corona after first elution), 4 (corona after second elution), and 5 (separation and refill after second elution).

investigated here, phosphate-buffered saline (PBS), combined with a slight pH shift also leads to an elution of around 65% of His_6-GFP bound to BIONs during the incubation. Slightly higher desorption rates can be observed using a common IMAC elution buffer based on a phosphate buffer containing NaCl and imidazole. However, the amount of imidazole does not affect desorption with decreasing concentrations from 500 to 50 mM. The results indicate that a clever manipulation of the system's electrostatic properties can lead to either a stable bound protein or an elution with unbound proteins. Considering the high binding capacity of His_6-GFP and the specific surface area of magnetic nanoparticles, there is only

DOI: 10.1021/acsomega.8b03348
ACS Omega 2019, 4, 3790−3799

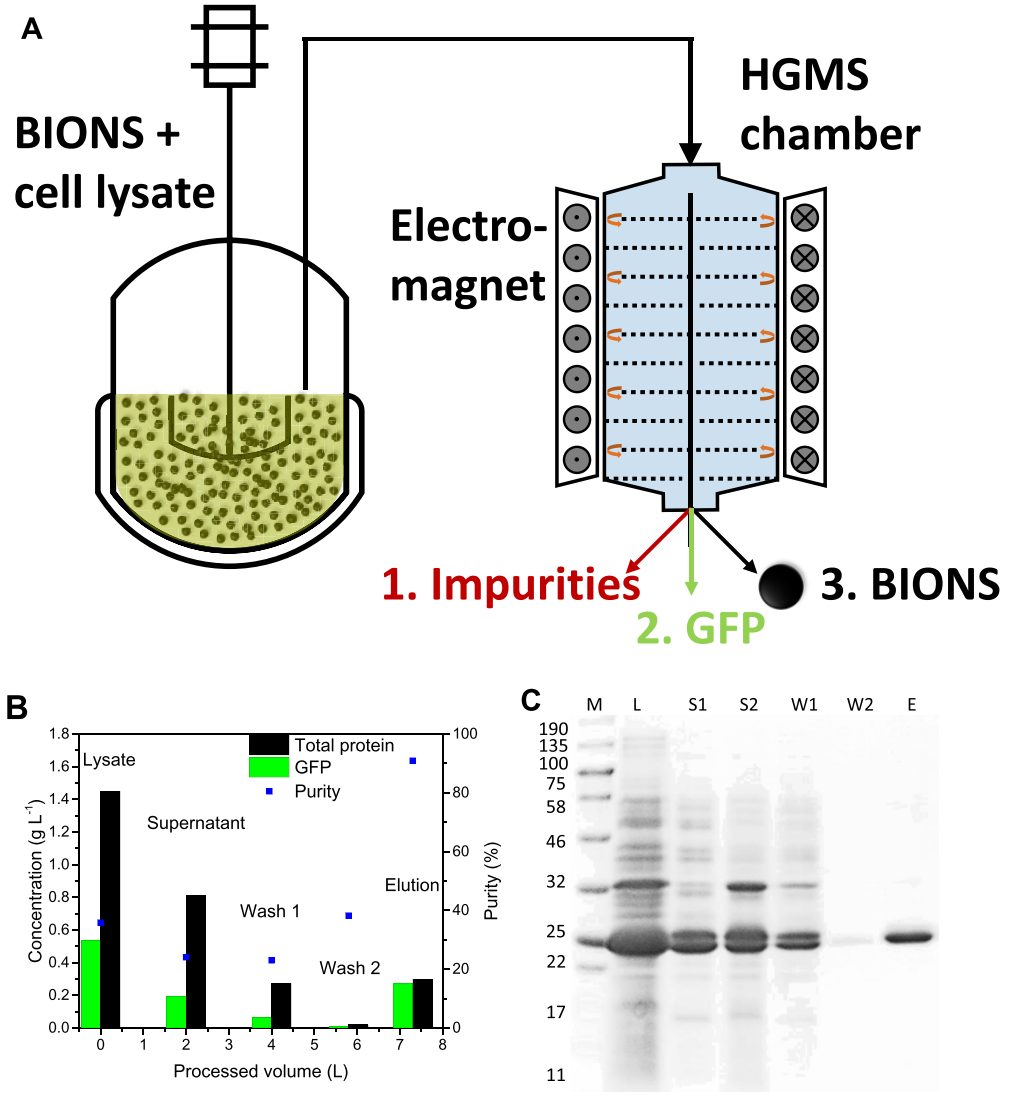

Figure 5. High-gradient magnetic fishing (HGMF) process for the purification of His_6-GFP. Cleared lysate (1 L) containing 1 g L^{-1} His_6-GFP and a total protein concentration of 3 g L^{-1} is mixed with a 1 L suspension containing BIONs. The whole system is buffered with Tris 50 mM at pH 7. After an incubation phase, particles and bound proteins are magnetically separated from the supernatant and washed two times, recirculating the suspension with 2 L of Tris buffer prior to elution with 500 mM imidazole IMAC buffer pH 7.5. (A) Schematic illustration of the separation process. (B) Total protein, GFP content, and GFP purity over the processing steps and the processed volume. (C) SDS-gel of all fractions collected during the process: M (marker: unstained protein marker, broad range (11−190 kDa)), L (cleared lysate diluted 1:2 in 50 mM Tris buffer pH 7), S1 (supernatant 1 diluted 1:1), S2 (supernatant 2 diluted 1:1), W1 (wash 1), W2 (wash 2), and E (eluate).

little space left for large cell fragments to also bind to the BION surface.

Protein adsorption to nanoparticles in complex media is usually a very fast process and the first surface layer is established after a few seconds.[17,63] From our observations, His_6-GFP behaves accordingly even considering the agglomeration of BIONs and thus no diffusion limitations can be observed.[64] However, the time span necessary for desorption processes is usually longer than for adsorption due to the different driving forces for adsorption and desorption.[65,66] Here, the His_6-GFP desorption was monitored over 1 day (Figure 3). For His-GFP bound to BIONs, incubation with the IMAC elution buffer leads to an immediate desorption (30 s) of around 10% proteins. After 5 min of incubation, around 30% of the protein can be desorbed and is found in the supernatant. With increasing incubation time, the amount of unbound GFP increases. The effect weakens with time, even though no stabilization of the elution maximum can be observed after 3 h. Most His_6-GFP is already desorbed after 30 min and around 70% is desorbed after an hour, with a maximal elution efficiency of 78% after 24 h (Figure 3A). The same behavior can be observed for purified His_6-GFP bound to BIONs and a His_6-GFP-containing cleared cell lysate bound within a protein corona around BIONs (Figure 3B). Possible explanations for this strongly time-dependent desorption behavior are the different diffusion behaviors for adsorption and elution as well as different adsorption and desorption kinetics.[65,66] Interestingly, no other protein can be observed with sodium dodecyl sulfate polyacrylamide gelelectrophoresis (SDS-PAGE) during the elution even though His_6-GFP at 27.8 kDa only accounts for 30% of the proteins in the cleared lysate (Figure 4A). Furthermore, no GFP dimers are visible in the elution fraction, which was the case after protein recovery from the IMAC column. Fluorescence microscopy also visually illustrates the

DOI: 10.1021/acsomega.8b03348
ACS Omega 2019, 4, 3790−3799

Table 1. Summary of Concentration, Mass, and Purity of His_6-GFP during the Different of the High-Gradient Magnetic Fishing Process as Well as the Purification Factor, Yield, and Concentration Factor for the Elution

samples	V (L)	c_{GFP} (g L^{-1})	m_{GFP} (g)	m_{Ges} (g)	P (%)	PF	Y (%)	CF
lysate	1	1.07	1.07	2.99	36			
supernatant	2	0.192	0.384	1.617	24			
wash 1	2	0.063	0.126	0.548	23			
wash 2	1.8	0.007	0.013	0.034	38			
elution	1.5	0.27	0.405	0.445	91	2.53	38	0.25

bound His_6-GFP on the BIONs (Figure 4B,C). Here, a slight decrease can be observed for the second elution step, whereas only a low amount of fluorescent components can be detected after an elution with IMAC buffer (Figure 4D). For the reference process with nontagged GFP, no binding can be detected with fluorescence microscopy and SDS-PAGE (Figures 4E and S8). However, whereas most of the protein can be recovered, some His_6-GFP is lost during the washing and some His_6-GFP remains bound even during two elution steps (Figure 4F). Furthermore, a second band occurs around 35 kDa in the SDS-PAGE of the cell lysate protein corona, which is not desorbed by the IMAC buffer. This band only occurs in the corona for incubation with His_6-GFP lysate and not for the nontagged GFP lysate. With matrix-assisted laser desorption ionization time-of-flight mass spectrometry, the outer membrane protein F (ompF) can be identified, which is responsible for the second band. The adsorption of ompF can be related to the similarities to GFP such as the β-barrel shape.[67] Furthermore, ompF contains many aspartate and glutamate subunits, which are mostly located at the terminal or peripheral sites of the protein, which are known to bind well to iron oxide nanoparticles.[61,67−69] Both lysates originate from the same *E. coli* strain, and this species cannot be detected in the elution fractions. Thus, this protein band is most likely a compound of His_6-GFP and other smaller proteins, which means that coadsorption with other proteins might actually improve the separation and recovery of His_6-GFP.

The simple application of a commercially available affinity tag by low-cost BIONs aroused our interest and we tried to implement a large-scale purification process with this system.[70] A rotor−stator separator (26 rotor and 25 stator plates) is used for the separation process. The sufficient magnetic field for the high-gradient magnetic fishing process is generated by an electromagnet (Figure S9). A magnetic flux of up to 0.6 T is induced by the magnet, which is in good agreement with a similar HGMF construction.[38] One liter of cleared lysate (1 g L^{-1} His_6-GFP) is mixed with 1 L BIONs (5.5 g L^{-1}) and then processed in an HGMF pilot separator (Figure 5A). The particles and bound proteins are magnetically separated from the supernatant and afterward redispersed in 2 L of binding buffer (50 mM Tris buffer pH 7) for two washing steps. The concentrations of the protein-containing lysate and BIONs were chosen comparable to the lab-scale experiments to ensure a proper ratio between particles and His_6-GFP and thus a reasonable upscaling of the process. However, a large amount of His_6-GFP is removed with the supernatant and in the first washing step (Figure 5B,C). Fluorescence measurements and SDS-PAGE of the different fractions match the optical observations (Table 1 and Figure S10). This loss can mainly be attributed to a pronounced foam formation during the redispersion with a moving rotor. Other reasons are losses in the tubing and separator chamber as well as difficulties with the upscaling of the magnetic separation and desorption process from the laboratory to liter scale. All these effects might influence the process significantly. However, the redispersion efficiency of magnetic particles in this rotor−stator HGMF separator is superior to that of static magnetizable matrices used for magnetic filtration.[39] Hence, a yield of 38% can still be reached with one elution using an IMAC buffer with only 50 mM imidazole content. The highlight of this process is the purity of 91%, which can be reached in this single-step purification, which accounts for a purification factor of 2.5 (Table S1). To our knowledge, no HGMF processes exist that lead to comparable results for the purification of a model protein with a His_6-tag by low-cost BIONs.

CONCLUSIONS

In summary, we demonstrated the manipulation of a protein corona originating from *E. coli* cell lysate around BIONs for the purification of a His_6-tagged model protein. A high affinity of the tag to BIONs can be verified for pure His_6-GFP solutions as well as for His_6-GFP in complex cell lysates. In most investigated buffer systems (acetate, MES, TBS, Tris), the established tag demonstrates a high affinity to the BION surface. Furthermore, high binding capacities of up to 50% surface coverage can be reached for His_6-tagged proteins, whereas a nontagged GFP does not show a high affinity and binding capacity to our particles. Thus, binding through the tag can be concluded, which can be substantiated with elution experiments where bound His_6-GFP can be eluted in a manner similar to that in commercially available IMAC columns. We combined these observations with a low-cost resource-friendly one-step purification process in the liter scale, which reaches a protein purity of 91%. Thus, we were able to demonstrate a successful upscaling of the process. However, these first proof of principle for the purification of His_6-tagged proteins with BIONs still meets many challenges. For industrially relevant processes, the loss of protein during adsorption and washing steps needs to be significantly reduced. Therefore, the tubing and the geometry of the separation chamber inlets and outlets should be improved, while foam formation needs to be suppressed during the whole process. Furthermore, the processing of higher protein and lysate concentrations and therefore of higher BION concentrations is desirable for more efficient processes. The recirculation of the supernatant as well as the reuse of nanoadsorbents is feasible; thus, this process can be operated with lower amounts of buffers and adsorbents and is therefore more sustainable than chromatographic techniques. Furthermore, no expensive functionalization with, or regeneration of, harmful metal ions is necessary. Consequently, this investigation might pave the way for new processing strategies based on magnetic separation principles for a greener downstream processing of proteins.

DOI: 10.1021/acsomega.8b03348
ACS Omega 2019, 4, 3790−3799

EXPERIMENTAL SECTION

All reagents used are commercially available, have a purity of >95% (high-performance liquid chromatography, HPLC grade), and were used as received without further purification. $FeCl_3 \cdot 6H_2O$ and sodium hydroxide were purchased from AppliChem GmbH, Germany, in the highest purity available. $FeCl_2 \cdot 4H_2O$ extra pure was obtained from Merck KGaA, Germany. The buffers are based on 50 mM phosphate, acetate, morpholino ethane sulfonic acid (MES), or tris-(hydroxymethyl)aminomethane (Tris) and double distilled water. Tris-buffered saline (TBS), citrate-buffered saline (CBS), and phosphate-buffered saline (PBS) contain additional 137 mM NaCl and 2.7 mM KCl, and 50 mM Tris, 50 mM citrate, and 50 mM phosphate, respectively. The imidazole elution buffer contains 500 mM NaCl, 50 mM $NaH_2PO_4 \cdot 2H_2O$, varying concentrations of imidazole between 50 and 500 mM, and double distilled water.

Magnetite was synthesized with a coprecipitation method described elsewhere.[42,55] Therefore, 21.2 g of $FeCl_3 \cdot 6H_2O$ and 8.29 g of $FeCl_2 \cdot 4H_2O$ were dissolved in 200 mL of deionized and degassed water. This iron chloride solution was added to 1 L of a 1 M solution of NaOH prepared with deionized and degassed water in a stirring tank reactor. The mixture was kept under nitrogen atmosphere for the whole reaction. The particles were washed several times with water.

His_6-GFP was overexpressed in *E. coli* BL21 (DE3) regulated by a T5 promotor in a 1000 L stirring tank reactor (Bioengineering AG, Wald, Switzerland). Bacteria were cultivated at 37 °C in Riesenberg medium in a fed-batch process, and the GFP expression was induced with isopropyl β-D-1-thiogalactopyranoside.[71] Cells were separated from the residual fermentation broth with a plate separator (CSA 08-06-476, GEA Westfalia Separator Group GmbH, Oelde). The lysis was conducted with a high-pressure homogenizer (Ariete NS3015H, GEA Niro Soavi, Parma IT), and the cell debris was separated with a depth filter (Z12DD 302 (3 M)).

Further downstream processing was only conducted to provide His_6-GFP with a purity of >99%. Therefore, a crossflow Sartoflow (Sartorius AG, Göttingen) equipped with Hydrosart 0.45 μm membranes (Sartorius) was used. This step was followed by anion-exchange chromatography (AEX) and an affinity chromatography step, where a HisTrap FF crude, loaded with a 5 mL nickel−nitrilo acid (Ni^{2+}−NTA) column, was used in an ÄKTApurifier System (GE Healthcare, Uppsala, SE). To change the buffer, protein solutions were washed with the respective new buffer several times in Vivaspin ultrafiltration spin columns (molecular weight cut-off 5k). The concentration was adjusted with bicinchoninic acid (BCA) assay and fluorescence measurements.

Adsorption and Elution Experiments. For the binding experiments, different amounts of His_6-GFP or lysate containing His_6-GFP were incubated with magnetite nanoparticles (1 g L^{-1}) at different concentrations in Tris buffer (50 mM, pH 7) for 1 h at 25 °C under vigorous shaking (1000 rpm). Even though the adsorption of proteins on nanoparticle surfaces depicts a dynamic equilibrium, for better comparison with other adsorption processes, the adsorption isotherms are fitted with the Langmuir equation.

$$q^* = \frac{q_{max} \cdot c^*}{K_D + c^*} \quad (1)$$

The surface coverage is calculated from q_{max} and the specific surface area S_m. Hereby, the specific surface area determined with the Brunauer−Emmett−Teller method is used. The density ρ of magnetite (5.2 g cm^{-3}) was used for the calculation.

For the surface coverage θ, the smallest area of the barrel-shaped GFP was considered (diameter 3 nm and height 4 nm).[10,72] His_6-GFP exhibits a molecular weight M_{GFP} of 27.8 kDa (SI).

$$\theta = \frac{q_{max} \cdot N_A \cdot \pi \left(\frac{d_{GFP}}{2}\right)^2}{S_m \cdot M_{GFP}} \quad (2)$$

To study the desorption kinetics, different incubation times were chosen, while an imidazole-containing IMAC elution buffer, TBS (50 mM, pH 9 or 5), PBS (50 mM, pH 7.4), or CBS (50 mM, pH 7) was used as the elution buffer. The supernatant was separated from the particles with hand magnets, decanted, and analyzed with an Infinite M200 Microplate Reader (Tecan Deutschland, Germany).

Protein Quantification. Supernatants from adsorption and elution experiments were further analyzed regarding their GFP content with fluorescence measurements, in an Infinite 200 Pro microplate reader (Tecan, Austria) at an excitation wavelength of 484 nm and detected at 515 nm, and HPLC.

For HPLC analysis of high-gradient magnetic separation experiments, a reverse-phase C4Aeris Widepore 3.6 μm, 100 × 2.1 mm^2 (Phenomenex, CA), was used at a flow rate of 0.2 mL min^{-1}. Samples were diluted to a GFP content below 0.5 g L^{-1} and filtered (0.2 μm) with a cellulose filter. A linear gradient from 40 to 70% acetonitrile (20 mM trifluoro acetic acid, TFA) with double distilled water (20 mM TFA) over 16 min was run for the separation of GFP from other proteins. The proteins were detected at 215 nm.

The total protein content was determined with a BCA assay (Pierce BCA Kit, Thermo Scientific, MA). The samples were diluted with the respective buffer.

The aliquots were further analyzed with sodium dodecyl sulfate polyacrylamide gelelectrophoresis (SDS-PAGE). Proteins were denatured at 95 °C for 5 min and stained with a Coomassie blue solution prior to loading on a 5% acrylamide stacking gel and run on a 15% separating gel under reducing conditions. Unstained protein marker (broad range, 2−212 kDa) was used as a reference. Here, 10 μL of the reference were applied, whereas 14 μL of the samples were used. All samples were applied undiluted unless stated otherwise.

For SDS-PAGE of the particle corona, samples were denatured at 100 °C for 5 min and stained with a Coomassie blue solution prior to loading on a 5% acrylamide stacking gel and run on a 10% separating gel under reducing conditions. Color protein standard broad range (10−250 kDa) was used as a reference. Here, 7.5 μL of the reference were applied, whereas 15 μL of the samples were used. All samples were applied in an undiluted state unless stated otherwise.

Fluorescence microscopy was conducted with an Andor (Nikon) spinning disk microscope equipped with a CFI Plan Apo 100× objective. Samples, which were diluted 1:10 with deionized water prior to analysis, were excited with a laser (488 nm), and the resulting emission was detected at 520 nm.

High-Gradient Magnetic Fishing (HGMF). The processing device comprises a stirred batch adsorption reactor equipped with a peristaltic pump, computer-controlled valves,

DOI: 10.1021/acsomega.8b03348
ACS Omega 2019, 4, 3790−3799

a bubble detector, and an associated stirrer. The electromagnet is water cooled and can generate a magnetic flux density of up to 0.25 T. The rotor−stator magnetic filter has a working volume of 980 mL and includes 25 stator and 26 rotor disks with an internal diameter of 86 mm. The maximum flow rate for the separator is 1400 mL min^{-1}. A flow rate of 200 mL min^{-1} was adjusted and used for the separation experiments. The residence time in the separation chamber for the experiments is 500 s. Particles are recovered from the separator by spinning the disks at a rotation speed of 1500 rpm.

Processing Steps. After incubation of the lysate and nanoparticles, the process includes a separation step, where the supernatant and the nanoparticles are separated magnetically, followed by two washing steps and an elution step.

Briefly, the cleared cell lysate containing 2.99 g protein with a His_6-GFP content of 32% is incubated with 11 g BIONs in 2 L of continuously stirred 50 mM Tris buffer (pH 7). The mixture is stirred at 1000 rpm for 60 min at room temperature prior to being pumped into the switched-on magnetic separator chamber. The supernatant is collected and analyzed, whereas the magnetic nanoparticles stick to the magnetized rotor and stator disks. The particles are backwashed with a new incubation buffer (50 mM Tris buffer pH 7) without magnetic field, but with a switched-on rotor, and circulated in the chamber before re-entering the chamber, which is again magnetized while the rotor is switched off. This procedure is repeated for the second wash step. For the elution, the particles containing bound GFP are pumped with the IMAC buffer (50 mM imidazole) to an external tank. Here, the elution is allowed for 1 h under vigorous stirring. After this procedure, the magnetic particles are backwashed again in Tris buffer. All fractions are collected and further analyzed concerning their GFP and protein content.

■ ASSOCIATED CONTENT

Supporting Information

The Supporting Information is available free of charge on the ACS Publications website at DOI: 10.1021/acsomega.8b03348.

Properties of BIONs: TEM image and particle size analysis, XRD, and Raman spectroscopy of BIONs; magnetic behavior of BIONs in different magnetic fields with SQUID; ζ-potential of BIONs; purification of His_6-GFP for pure protein experiments; IMAC runs and summary of protein purity from HPLC analysis; summary of binding capacity/load, affinity, ligand density, and surface coverage from pure protein adsorption isotherms; dynamic light scattering, differential centrifugal sedimentation, and optical centrifugation of particle agglomerates; simulation of magnetic fields in the high-gradient magnetic separator chamber; images of collected fractions (PDF)

■ AUTHOR INFORMATION

Corresponding Authors

*E-mail: S.Schwaminger@tum.de (S.P.S.).
*E-mail: P.Fraga@tum.de (P.F.-G.).
*E-mail: S.Berensmeier@tum.de (S.B.).

ORCID

Sebastian P. Schwaminger: 0000-0002-8627-0807
Silvia A. Blank-Shim: 0000-0003-0239-8545
Kenneth A. Dawson: 0000-0002-0568-6588

Author Contributions

This manuscript was written through contributions of all authors. All authors have given approval to the final version of the manuscript.

Author Contributions

‖S.P.S. and P.F.-G. contributed equally to this work.

Notes

The authors declare no competing financial interest.

■ ACKNOWLEDGMENTS

We thank Dr Dominik Maslak for the use of the TUM Research Center for Industrial Biotechnology and the provision with cell lysate. Furthermore, we would like to thank Dr Teodora Miclaus for DCS measurements and Marina Rottmüller for help with the manuscript. We are particularly appreciative of the financial support for this work by the Federal Ministry of Education and Research (Grant number 031A173A). We appreciate support from the German Research Foundation (DFG) and the Technical University of Munich (TUM) in the framework of the Open-Access Publishing Program.

■ REFERENCES

(1) Li, Y.; Xu, Y.; Fleischer, C. C.; Huang, J.; Lin, R.; Yang, L.; Mao, H. Impact of Anti-Biofouling Surface Coatings on the Properties of Nanomaterials and their Biomedical Applications. *J. Mater. Chem. B* **2018**, *6*, 9−24.

(2) Nosrati, H.; Rashidi, N.; Danafar, H.; Manjili, H. K. Anticancer Activity of Tamoxifen Loaded Tyrosine Decorated Biocompatible Fe_3O_4 Magnetic Nanoparticles against Breast cancer Cell Lines. *J. Inorg. Organomet. Polym.* **2017**, *13*, 101.

(3) Lee, N.; Hyeon, T. Designed Synthesis of Uniformly Sized Iron Oxide Nanoparticles for Efficient Magnetic Resonance Imaging Contrast Agents. *Chem. Soc. Rev.* **2012**, *41*, 2575−2589.

(4) Mikhaylov, G.; Mikac, U.; Magaeva, A. A.; Itin, V. I.; Naiden, E. P.; Psakhye, I.; Babes, L.; Reinheckel, T.; Peters, C.; Zeiser, R.; Bogyo, M.; Turk, V.; Psakhye, S. G.; Turk, B.; Vasiljeva, O. Ferri-Liposomes as an MRI-visible Drug-Delivery System for Targeting Tumours and their Microenvironment. *Nat. Nanotechnol.* **2011**, *6*, 594−602.

(5) Turner, A. P. F. Biosensors: Sense and Sensibility. *Chem. Soc. Rev.* **2013**, *42*, 3184−3196.

(6) Zhao, W.-W.; Xu, J.-J.; Chen, H.-Y. Photoelectrochemical DNA Biosensors. *Chem. Rev.* **2014**, *114*, 7421−7441.

(7) Polshettiwar, V.; Luque, R.; Fihri, A.; Zhu, H.; Bouhrara, M.; Basset, J.-M. Magnetically Recoverable Nanocatalysts. *Chem. Rev.* **2011**, *111*, 3036−3075.

(8) Roth, H.-C.; Schwaminger, S. P.; Peng, F.; Berensmeier, S. Immobilization of Cellulase on Magnetic Nanocarriers. *ChemistryOpen* **2016**, *5*, 183−187.

(9) Liu, G.; Gao, J.; Ai, H.; Chen, X. Applications and Potential Toxicity of Magnetic Iron Oxide Nanoparticles. *Small* **2013**, *9*, 1533−1545.

(10) Xia, S.; Cartron, M.; Morby, J.; Bryant, D. A.; Hunter, C. N.; Leggett, G. J. Fabrication of Nanometer- and Micrometer-Scale Protein Structures by Site-Specific Immobilization of Histidine-Tagged Proteins to Aminosiloxane Films with Photoremovable Protein-Resistant Protecting Groups. *Langmuir* **2016**, *32*, 1818−1827.

(11) Zhou, J.; Liang, Y.; He, X.; Chen, L.; Zhang, Y. Dual-Functionalized Magnetic Metal−Organic Framework for Highly Specific Enrichment of Phosphopeptides. *ACS Sustainable Chem. Eng.* **2017**, *5*, 11413−11421.

(12) Colombo, M.; Carregal-Romero, S.; Casula, M. F.; Gutiérrez, L.; Morales, M. P.; Böhm, I. B.; Heverhagen, J. T.; Prosperi, D.; Parak, W. J. Biological Applications of Magnetic Nanoparticles. *Chem. Soc. Rev.* **2012**, *41*, 4306−4334.

DOI: 10.1021/acsomega.8b03348
ACS Omega 2019, 4, 3790−3799

(13) Mahmoudi, M.; Lynch, I.; Ejtehadi, M. R.; Monopoli, M. P.; Bombelli, F. B.; Laurent, S. Protein-Nanoparticle Interactions: Opportunities and Challenges. *Chem. Rev.* **2011**, *111*, 5610−5637.
(14) Schwaminger, S.; Blank-Shim, S. A.; Borkowska-Panek, M.; Anand, P.; Fraga-García, P.; Fink, K.; Wenzel, W.; Berensmeier, S. Experimental Characterization and Simulation of Amino Acid and Peptide Interactions with Inorganic Materials. *Eng. Life Sci.* **2018**, *18*, 84−100.
(15) Maiolo, D.; Bergese, P.; Mahon, E.; Dawson, K. A.; Monopoli, M. P. Surfactant Titration of Nanoparticle-Protein Corona. *Anal. Chem.* **2014**, *86*, 12055−12063.
(16) Cedervall, T.; Lynch, I.; Foy, M.; Berggård, T.; Donnelly, S. C.; Cagney, G.; Linse, S.; Dawson, K. A. Detailed Identification of Plasma Proteins Adsorbed on Copolymer Nanoparticles. *Angew. Chem., Int. Ed.* **2007**, *46*, 5754−5756.
(17) Cedervall, T.; Lynch, I.; Lindman, S.; Berggård, T.; Thulin, E.; Nilsson, H.; Dawson, K. A.; Linse, S. Understanding the Nanoparticle-Protein Corona Using Methods to Quantify Exchange Rates and Affinities of Proteins for Nanoparticles. *Proc. Natl. Acad. Sci. U.S.A.* **2007**, *104*, 2050−2055.
(18) Lynch, I.; Dawson, K. A. Protein-Nanoparticle Interactions. *Nano Today* **2008**, *3*, 40−47.
(19) Mahon, E.; Salvati, A.; Baldelli Bombelli, F.; Lynch, I.; Dawson, K. A. Designing the Nanoparticle-Biomolecule Interface for "Targeting and Therapeutic Delivery". *J. Controlled Release* **2012**, *161*, 164−174.
(20) Monopoli, M. P.; Aberg, C.; Salvati, A.; Dawson, K. A. Biomolecular Coronas Provide the Biological Identity of Nanosized Materials. *Nat. Nanotechnol.* **2012**, *7*, 779−786.
(21) Lu, A.-H.; Salabas, E. L.; Schüth, F. Magnetic Nanoparticles: Synthesis, Protection, Functionalization, and Application. *Angew. Chem., Int. Ed.* **2007**, *46*, 1222−1244.
(22) Laurent, S.; Forge, D.; Port, M.; Roch, A.; Robic, C.; Vander Elst, L.; Muller, R. N. Magnetic Iron Oxide Nanoparticles: Synthesis, Stabilization, Vectorization, Physicochemical Characterizations, and Biological Applications. *Chem. Rev.* **2008**, *108*, 2064−2110.
(23) Qiao, R.; Yang, C.; Gao, M. Superparamagnetic Iron Oxide Nanoparticles: From Preparations to in vivo MRI Applications. *J. Mater. Chem.* **2009**, *19*, 6274.
(24) Pan, Y.; Du, X.; Zhao, F.; Xu, B. Magnetic Nanoparticles for the Manipulation of Proteins and Cells. *Chem. Soc. Rev.* **2012**, *41*, 2912−2942.
(25) Schwaminger, S. P.; Fraga-García, P.; Selbach, F.; Hein, F. G.; Fuß, E. C.; Surya, R.; Roth, H.-C.; Blank-Shim, S. A.; Wagner, F. E.; Heissler, S.; Berensmeier, S. Bio-Nano Interactions: Cellulase on Iron Oxide Nanoparticle Surfaces. *Adsorption* **2017**, *23*, 281−292.
(26) Dineshkumar, R.; Paul, A.; Gangopadhyay, M.; Singh, N. D. P.; Sen, R. Smart and Reusable Biopolymer Nanocomposite for Simultaneous Microalgal Biomass Harvesting and Disruption: Integrated Downstream Processing for a Sustainable Biorefinery. *ACS Sustainable Chem. Eng.* **2017**, *5*, 852−861.
(27) Reddy, L. H.; Arias, J. L.; Nicolas, J.; Couvreur, P. Magnetic Nanoparticles: Design and Characterization, Toxicity and Biocompatibility, Pharmaceutical and Biomedical Applications. *Chem. Rev.* **2012**, *112*, 5818−5878.
(28) Gomes, C. S. G.; Fashina, A.; Fernández-Castané, A.; Overton, T. W.; Hobley, T. J.; Theodosiou, E.; Thomas, O. R. T. Magnetic Hydrophobic-Charge Induction Adsorbents for the Recovery of Immunoglobulins from Antiserum Feedstocks by High-Gradient Magnetic Fishing. *J. Chem. Technol. Biotechnol.* **2018**, *93*, 1901−1915.
(29) Gawande, M. B.; Branco, P. S.; Varma, R. S. Nano-Magnetite (Fe_3O_4) as a Support for Recyclable Catalysts in the Development of Sustainable Methodologies. *Chem. Soc. Rev.* **2013**, *42*, 3371−3393.
(30) Reiss, G.; Hütten, A. Magnetic Nanoparticles: Applications Beyond Data Storage. *Nat. Mater.* **2005**, *4*, 725−726.
(31) Röder, R.; Preiß, T.; Hirschle, P.; Steinborn, B.; Zimpel, A.; Höhn, M.; Rädler, J. O.; Bein, T.; Wagner, E.; Wuttke, S.; Lächelt, U. Multifunctional Nanoparticles by Coordinative Self-Assembly of His-Tagged Units with Metal-Organic Frameworks. *J. Am. Chem. Soc.* **2017**, *139*, 2359−2368.
(32) Wei, X.; Duan, J.; Xu, X.; Zhang, L. Highly Efficient One-Step Purification of Sulfated Polysaccharides via Chitosan Microspheres. *ACS Sustainable Chem. Eng.* **2017**, *5*, 3195−3203.
(33) Boselli, L.; Polo, E.; Castagnola, V.; Dawson, K. A. Regimes of Biomolecular Ultrasmall Nanoparticle Interactions. *Angew. Chem., Int. Ed.* **2017**, *56*, 4215−4218.
(34) Rabe, M.; Verdes, D.; Seeger, S. Understanding Protein Adsorption Phenomena at Solid Surfaces. *Adv. Colloid Interface Sci.* **2011**, *162*, 87−106.
(35) Salvati, A.; Pitek, A. S.; Monopoli, M. P.; Prapainop, K.; Bombelli, F. B.; Hristov, D. R.; Kelly, P. M.; Åberg, C.; Mahon, E.; Dawson, K. A. Transferrin-Functionalized Nanoparticles Lose their Targeting Capabilities when a Biomolecule Corona Adsorbs on the Surface. *Nat. Nanotechnol.* **2013**, *8*, 137−143.
(36) Pettibone, J. M.; Cwiertny, D. M.; Scherer, M.; Grassian, V. H. Adsorption of Organic Acids on TiO_2 Nanoparticles: Effects of pH, Nanoparticle Size, and Nanoparticle Aggregation. *Langmuir* **2008**, *24*, 6659−6667.
(37) Kolhatkar, A. G.; Jamison, A. C.; Litvinov, D.; Willson, R. C.; Lee, T. R. Tuning the Magnetic Properties of Nanoparticles. *Int. J. Mol. Sci.* **2013**, *14*, 15977−16009.
(38) Ebeler, M.; Pilgram, F.; Wolz, K.; Grim, G.; Franzreb, M. Magnetic Separation on a New Level: Characterization and Performance Prediction of a cGMP Compliant "Rotor-Stator" High-Gradient Magnetic Separator. *Biotechnol. J.* **2018**, *13*, No. 1700448.
(39) Roth, H.-C.; Prams, A.; Lutz, M.; Ritscher, J.; Raab, M.; Berensmeier, S. A High-Gradient Magnetic Separator for Highly Viscous Process Liquors in Industrial Biotechnology. *Chem. Eng. Technol.* **2016**, *39*, 469−476.
(40) Schwaminger, S. P.; Surya, R.; Filser, S.; Wimmer, A.; Weigl, F.; Fraga-García, P.; Berensmeier, S. Formation of Iron Oxide Nanoparticles for the Photooxidation of Water: Alteration of Finite Size Effects from Ferrihydrite to Hematite. *Sci. Rep.* **2017**, *7*, No. 12609.
(41) Fraga García, P.; Freiherr von Roman, M.; Reinlein, S.; Wolf, M.; Berensmeier, S. Impact of Nanoparticle Aggregation on Protein Recovery Through a Pentadentate Chelate Ligand on Magnetic Carriers. *ACS Appl. Mater. Interfaces* **2014**, *6*, 13607−13616.
(42) Schwaminger, S. P.; Bauer, D.; Fraga-García, P.; Wagner, F. E.; Berensmeier, S. Oxidation of Magnetite Nanoparticles: Impact on Surface and Crystal Properties. *CrystEngComm* **2017**, *19*, 246−255.
(43) Roth, H.-C.; Schwaminger, S. P.; Schindler, M.; Wagner, F. E.; Berensmeier, S. Influencing Factors in the Co-Precipitation Process of Superparamagnetic Iron Oxide Nano particles: A Model Based Study. *J. Magn. Magn. Mater.* **2015**, *377*, 81−89.
(44) Tombácz, E.; Hajdú, A.; Illés, E.; László, K.; Garberoglio, G.; Jedlovszky, P. Water in Contact with Magnetite Nanoparticles, as Seen from Experiments and Computer Simulations. *Langmuir* **2009**, *25*, 13007−13014.
(45) Porath, J.; Carlsson, J. A.; Olsson, I.; Belfrage, G. Metal Chelate Affinity Chromatography, a New Approach to Protein Fractionation. *Nature* **1975**, *258*, 598.
(46) Porath, J. Immobilized Metal Ion Affinity Chromatography. *Protein Expression Purif.* **1992**, *3*, 263−281.
(47) Fraga García, P.; Brammen, M.; Wolf, M.; Reinlein, S.; Freiherr von Roman, M.; Berensmeier, S. High-Gradient Magnetic Separation for Technical Scale Protein Recovery Using Low Cost Magnetic Nanoparticles. *Sep. Purif. Technol.* **2015**, *150*, 29−36.
(48) Safarik, I.; Safarikova, M. Magnetic Techniques for the Isolation and Purification of Proteins and Peptides. *Biomagn. Res. Technol.* **2004**, *2*, 7.
(49) Xu, F.; Geiger, J. H.; Baker, G. L.; Bruening, M. L. Polymer Brush-Modified Magnetic Nanoparticles for His-Tagged Protein Purification. *Langmuir* **2011**, *27*, 3106−3112.
(50) Shao, M.; Ning, F.; Zhao, J.; Wei, M.; Evans, D. G.; Duan, X. Preparation of Fe3O4@SiO2@Layered Double Hydroxide Core-Shell Microspheres for Magnetic Separation of Proteins. *J. Am. Chem. Soc.* **2012**, *134*, 1071−1077.

DOI: 10.1021/acsomega.8b03348
ACS Omega 2019, 4, 3790−3799

(51) Franzreb, M.; Siemann-Herzberg, M.; Hobley, T. J.; Thomas, O. R. T. Protein Purification Using Magnetic Adsorbent Particles. *Appl. Microbiol. Biotechnol.* **2006**, *70*, 505−516.
(52) Blank-Shim, S. A.; Schwaminger, S. P.; Borkowska-Panek, M.; Anand, P.; Yamin, P.; Fraga-García, P.; Fink, K.; Wenzel, W.; Berensmeier, S. Binding Patterns of Homo-Peptides on Bare Magnetic Nanoparticles: Insights into Environmental Dependence. *Sci. Rep.* **2017**, *7*, No. 14047.
(53) Kupcik, R.; Rehulka, P.; Bilkova, Z.; Sopha, H.; Macak, J. M. New Interface for Purification of Proteins: One-Dimensional TiO_2 Nanotubes Decorated by Fe_3O_4 Nanoparticles. *ACS Appl. Mater. Interfaces* **2017**, *9*, 28233−28242.
(54) Block, H.; Maertens, B.; Spriestersbach, A.; Brinker, N.; Kubicek, J.; Fabis, R.; Labahn, J.; Schäfer, F. Immobilized-Metal Affinity Chromatography (IMAC). In *Methods in Enzymology*; Guide to Protein Purification; 2nd ed.; Burgess, R. R., Deutscher, M. P., Eds.; Elsevier Academic Press: San Diego, CA, 2009; Vol. *463*, pp 439−473.
(55) Schwaminger, S. P.; Blank-Shim, S. A.; Scheifele, I.; Fraga-García, P.; Berensmeier, S. Peptide Binding to Metal Oxide Nanoparticles. *Faraday Discuss.* **2017**, *204*, 233−250.
(56) Cugia, F.; Sedda, S.; Pitzalis, F.; Parsons, D. F.; Monduzzi, M.; Salis, A. Are Specific Buffer Effects the New Frontier of Hofmeister Phenomena?: Insights from Lysozyme Adsorption on Ordered Mesoporous Silica. *RSC Adv.* **2016**, *6*, 94617−94621.
(57) dos Santos, A. P.; Levin, Y. Surface and Interfacial Tensions of Hofmeister Electrolytes. *Faraday Discuss.* **2013**, *160*, 75−87 discussion 103-20. .
(58) Lata, S.; Reichel, A.; Brock, R.; Tampé, R.; Piehler, J. High-Affinity Adaptors for Switchable Recognition of Histidine-Tagged Proteins. *J. Am. Chem. Soc.* **2005**, *127*, 10205−10215.
(59) Baalousha, M. Aggregation and Disaggregation of Iron Oxide Nanoparticles: Influence of Particle Concentration, pH and Natural Organic Matter. *Sci. Total Environ.* **2009**, *407*, 2093−2101.
(60) Vindedahl, A. M.; Strehlau, J. H.; Arnold, W. A.; Penn, R. L. Organic Matter and Iron Oxide Nanoparticles: Aggregation, Interactions, and Reactivity. *Environ. Sci.: Nano* **2016**, *3*, 494−505.
(61) Schwaminger, S. P.; Blank-Shim, S. A.; Scheifele, I.; Pipich, V.; Fraga-García, P.; Berensmeier, S. Design of Interactions between Nanomaterials and Proteins: A Highly Affine Peptide Tag Bare Iron Oxide Nanoparticles for Magnetic Protein Separation. *Biotechnol. J.* **2018**, No. e1800055.
(62) Moerz, S. T.; Huber, P. Protein Adsorption into Mesopores: A Combination of Electrostatic Interaction, Counterion Release, and van der Waals Forces. *Langmuir* **2014**, *30*, 2729−2737.
(63) Tenzer, S.; Docter, D.; Kuharev, J.; Musyanovych, A.; Fetz, V.; Hecht, R.; Schlenk, F.; Fischer, D.; Kiouptsi, K.; Reinhardt, C.; Landfester, K.; Schild, H.; Maskos, M.; Knauer, S. K.; Stauber, R. H. Rapid Formation of Plasma Protein Corona Critically Affects Nanoparticle Pathophysiology. *Nat. Nanotechnol.* **2013**, *8*, 772−781.
(64) Zhdanov, V. P.; Kasemo, B. Diffusion-Limited Kinetics of Adsorption of Biomolecules on Supported Nanoparticles. *Colloids Surf., B* **2010**, *76*, 28−31.
(65) Kiesel, I.; Paulus, M.; Nase, J.; Tiemeyer, S.; Sternemann, C.; Rüster, K.; Wirkert, F. J.; Mende, K.; Büning, T.; Tolan, M. Temperature-Driven Adsorption and Desorption of Proteins at Solid-Liquid Interfaces. *Langmuir* **2014**, *30*, 2077−2083.
(66) Miller, R.; Grigoriev, D.; Kragel, J.; Makievski, A.; Maldonado-Valderrama, J.; Leser, M.; Michel, M.; Fainerman, V. Experimental Studies on the Desorption of Adsorbed Proteins from Liquid Interfaces. *Food Hydrocolloids* **2005**, *19*, 479−483.
(67) Cowan, S. W.; Schirmer, T.; Rummel, G.; Steiert, M.; Ghosh, R.; Pauptit, R. A.; Jansonius, J. N.; Rosenbusch, J. P. Crystal Structures Explain Functional Properties of Two E. coli Porins. *Nature* **1992**, *358*, 727−733.
(68) Berensmeier, S.; Blank-Shim, S. A.; Schwaminger, S. P.; Fraga-García, P.; Wenzel, W.; Fink, K.; Anand, P.; Borkowska-Panek, M. Magnetic-Particle Binding Peptides. WO Patent WO2018050826A1, 2016.
(69) Yamashita, E.; Zhalnina, M. V.; Zakharov, S. D.; Sharma, O.; Cramer, W. A. Crystal Structures of the OmpF Porin: Function in a Colicin Translocon. *EMBO J.* **2008**, *27*, 2171−2180.
(70) Lichty, J. J.; Malecki, J. L.; Agnew, H. D.; Michelson-Horowitz, D. J.; Tan, S. Comparison of Affinity Tags for Protein Purification. *Protein Expression Purif.* **2005**, *41*, 98−105.
(71) Riesenberg, D.; Schulz, V.; Knorre, W. A.; Pohl, H.-D.; Korz, D.; Sanders, E. A.; Roß, A.; Deckwer, W.-D. High Cell Density Cultivation of Escherichia coli at Controlled Specific Growth Rate. *J. Biotechnol.* **1991**, *20*, 17−27.
(72) Orm, M.; Cubitt, A. B.; Kallio, K.; Gross, L. A.; Tsien, R. Y.; Remington, S. J. Crystal Structure of the Aequorea victoria Green Fluorescent Protein. *Science* **1996**, *273*, 1392−1395.

DOI: 10.1021/acsomega.8b03348
ACS Omega 2019, 4, 3790−3799